Environmental and Experimental Botany 71 (2011) 232–240

Contents lists available at ScienceDirect

Environmental and Experimental Botany

journal homepage: www.elsevier.com/locate/envexpbot

Dimethylglyoxime (DMG) staining for semi-quantitative mapping of Ni in plant tissue

Anja Gramlich[a,*], Ahmad B. Moradi[b], Brett H. Robinson[c], Anders Kaestner[d], Rainer Schulin[a]

[a] Institute of Terrestrial Ecosystems, ETH, Universitätstr. 16, CH-8092 Zurich, Switzerland
[b] Helmholtz Centre for Environmental Research - UFZ, Leipzig, Germany
[c] Agriculture and Life Sciences Division, Lincoln University, Canterbury, New Zealand
[d] Paul Scherrer Institut, Villigen, Switzerland

ARTICLE INFO

Article history:
Received 23 July 2010
Received in revised form 15 October 2010
Accepted 6 December 2010

Keywords:
Ni hyperaccumulator
Dimethylglyoxime (DMG)
Semi-quantitative Ni staining
Berkheya coddii

ABSTRACT

Determination of the nickel (Ni) distribution in tissues of hyperaccumulator plants aids in understanding the strategies and mechanisms used by these plants to take up Ni from soils. Commonly used methods for measuring Ni distribution in plant tissues require expensive equipment and complex sample preparation. We tested a suite of staining methods consisting of dimethylglyoxime (DMG) dissolved in a range of solvents for the mapping of Ni distribution in the Ni hyperaccumulator *Berkheya coddii Roessler*. The best solution was DMG (10 g l^{-1}) dissolved in borax (25 mM) and KOH (30 mM). Plant tissue cross-sections were imaged under a microscope immediately after DMG application. A Karhunen–Loeve transformation was applied to the images to minimize interference from colours of other origin, e.g. from chlorophyll. The distribution of Ni could be determined at the cellular level and consistent patterns were obtained for replicates. Staining of Ni dissolved in agar at various concentrations was used to calibrate the method. Concentrations as low as 50 mg kg^{-1} (fresh weight) could be detected. Averaged over several cross-sections the DMG method systematically gave lower concentrations than ICP-OES analysis of the respective plant part, indicating that not all Ni in the tissue reacted with DMG, but only Ni that is readily available. The DMG method may be used in conjunction with spectroscopic methods to resolve biologically active Ni.

1. Introduction

Soils derived from ultramafic (serpentine) rocks naturally contain high concentrations of nickel (Ni), usually in the range 0.1–3% Ni (Brooks, 1987). Some plants spontaneously occurring on these soils accumulate one or more orders of magnitude more Ni in their shoots than other species growing in the same environment (Brooks et al., 1977). Plants that accumulate >1000 mg of a trace element kg^{-1} (dry weight), concentrating the element more in the shoot than in the roots, are called hyperaccumulators. There are more than 300 known species of Ni hyperaccumulators, belonging to more than 33 families (Brooks, 1998b). As the toxicity of the accumulated Ni must be controlled, hyperaccumulation comes at a metabolic cost for the plant, which would be avoided if the metal would be excluded from being taken up by the roots and translocated into the shoots. It is hypothesised that hyperaccumulation confers benefits to the plant, including increased protection against herbivores (Boyd, 1998; Robinson et al., 2003; Sagner et al., 1998). Studies on the distribution of Ni and other heavy metals in plant tissues can provide important information on the mechanisms and ecological benefits of hyperaccumulation. For example, protection against phloem-sucking insects will only be effective if Ni is present at sufficiently high concentrations in the phloem. Understanding Ni allocation in various plant parts can also be valuable for the development of methods using plants to clean up Ni-contaminated soils or for the assessment of risks arising from the use of such soils for crop production (McNear et al., 2005). Soil contamination by Ni can arise from the deposition of dusts generated by mining and smelting activities, shooting, and land application of sewage sludge (Robinson et al., 1997; Brooks, 1998a; Migliorini et al., 2004).

Many authors have studied the distribution of metals in hyperaccumulator plants using electron dispersive X-ray analysis (EDXA) (e.g. Robinson et al., 2003; Bidwell et al., 2004; Marmiroli et al., 2004; Berazain et al., 2007). Unfortunately, EDXA is limited to Ni metal concentrations above 1000 mg kg^{-1} dry weight (McNear et al., 2005). Critical in EDXA analysis is the position of the sample relative to the X-ray beam during analysis. Large errors can occur if the angle between sample and beam is not precisely controlled. Another source of error is interferences of the energy emission lines of the target element with other elements present in the

* Corresponding author. Tel.: +41 44 632 84 60.
E-mail address: anja.gramlich@env.ethz.ch (A. Gramlich).

0098-8472/$ – see front matter © 2010 Elsevier B.V. All rights reserved.
doi:10.1016/j.envexpbot.2010.12.008

sample. Moreover, artefacts may result from Ni redistribution in or leaching from non-frozen samples. Mesjasz-Przybylowicz et al. (2001), Bhatia et al. (2004) and Budka et al. (2005) quantified Ni concentrations in various leaf tissues at cellular level using micro-proton-induced X-ray emission spectroscopy (micro-PIXE), which has a detection limit of 1–10 mg kg^{-1} dehydrated samples (Ortega, 2005). Micro-PIXE analyses are performed under vacuum on thin sections of resin-embedded samples. Thereby, Ni redistribution offsets some of the gain in sensitivity. Budka et al. (2005) tested several media for freeze-substitution and showed that the distributions and concentrations of metal were heavily dependent on the medium.

Smart et al. (2007) used high-resolution secondary ion mass spectroscopy (NanoSIMS) for analysing Ni distribution in leaf tissues. This technique can quantify metals at the sub-cellular level due to its high spatial resolution (0.05 μm). A further advantage is the low detection limit of <0.1 mg kg^{-1} for dehydrated samples (Ortega, 2005). However, it requires a complex chemical pre-treatment of the sample that may result in Ni redistribution. McNear et al. (2005) used synchrotron-based fluorescence computed microtomography (CMT) and synchrotron-based absorption-edge CMT to investigate the distribution of Ni in *Alyssum murale*. These techniques have the advantage that they can provide 3D images without sectioning the sample, while the detection limits are still reasonably low (<18–37 mg Ni kg^{-1} dry weight). However, the samples need to be shock-frozen and dried. Therefore, a truly in vivo analysis in many cases is impossible. Another drawback of microPIXE, nanoSIMS and synchrotron-based CMT techniques is that they involve a high level of expertise and complex facilities to which access is limited.

1.1. Dimethylglyoxime (DMG) analysis

Element-specific staining techniques do not require expensive and complex equipment. Various authors have used such techniques to localize metals in plant tissues. Tung and Temple (1996) conducted histochemical studies on the distribution of lead (Pb) in root, stem and leaf tissues of various plant species using sodium rhodizonate as a staining agent. Andreĭ et al. (2006) and Ozturk et al. (2006) investigated the zinc (Zn) distribution in sycamore maple leaves and in seeds of wheat plants, respectively, by element specific staining techniques. Dimethylglyoxime (DMG) is a staining agent particularly well suited for Ni. DMG forms strong complexes with Ni. The Ni–DMG complex reflects and transmits red light in the range of 600–450 nm (Dakhel et al., 2006). This colouration can reveal the distribution of Ni in plant tissues. Interferences may occur with cadmium (Cd) and copper (Cu), which also form red complexes with DMG. The colour of the latter complexes, however, is less intense than that of $Ni(DMG)_2$. At concentrations that normally occur in Ni hyperaccumulator plant tissues, Cd and Cu staining by DMG is negligible in comparison to Ni (Seregin et al., 2003).

Many investigators have used DMG for qualitative microscopic detection of Ni in plant tissues (L'Huillier et al., 1996; Heath et al., 1997; Sagner et al., 1998; Küpper et al., 2001; Boominathan and Doran, 2003; Mizuno et al., 2003; Seregin et al., 2003; Bhatia et al., 2004; Richau et al., 2009). Some authors reported crystal formation and Ni redistribution (Bhatia et al., 2004; Mizuno et al., 2003). Whether such artefacts are a problem, however, depends on sample preparation and the type of DMG solution. As DMG is only sparingly soluble in water, ethanol-containing solutions are often used. Ethanol was found to enhance the penetration of some tissues by DMG (Smart et al., 2007), but also to destroy tissue structure and thus may contribute to Ni redistribution (Seregin et al., 2003).

The time over which cross-sections are exposed to the DMG-solutions plays an important role in DMG staining. Seregin et al. (2003) found that the formation of crystals was no problem if the tissues were imaged immediately after DMG staining. Another advantage of rapid imaging is that there is less time for Ni redistribution in the tissue. However, only a fraction of the reactive Ni may be complexed if the exposure time is too short. Thus, there is a trade-off between the risk of artefacts and the completeness of Ni detection.

No attempts have been made (or at least published) to use DMG staining in order to determine the distribution of Ni in plant tissues quantitatively. The aim of this study was to develop a method that could be used to determine at least semi-quantitatively the distribution of Ni in hyperaccumulator plants at tissue level. In particular, we sought (1) an appropriate DMG solvent for application to plant tissue, (2) to quantify the intensity of the DMG stain using image analysis, (3) to map Ni concentrations across root, shoot and leaf sections at tissue level, and (4) to validate the method by comparing tissue Ni concentrations determined by DMG staining with tissue analysis by inductively coupled plasma optical emission spectroscopy (ICP-OES).

2. Materials and methods

2.1. Plant cultivation

We germinated seeds of *B. coddii*, a well-known Ni hyperaccumulator of the *Asteraceae* family, and grew the seedlings for three weeks in perlite. The seedlings were then transferred to 0.3 l pots filled with a sandy soil (sand:silt:clay-ratio: 87:8:5) with a pH of 6.4 (KCl), collected from the subsoil of a forest of Eiken, Switzerland. The organic carbon content was 0.6%. The Ni concentration in the unspiked soil was analysed using X-ray fluorescence spectroscopy (XRF, X-Lab 2000, Spectro, Kleve, Germany). Before filling into the pots, $Ni(NO_3)_2$ was added to the soil to produce the following concentrations: 0 (control), 31.25, 62.5, 125, 250 and 500 mg Ni kg^{-1} soil. Three replicate pots were prepared for each Ni concentration. After two months in a climate chamber (with a daily light cycle of 16 h light/8 h darkness, constant humidity of 75%, and controlled variation in temperature between 23 °C during day and 16 °C over night), we took fresh samples from leaves, roots and stem tissues for cross-sectioning and DMG staining. The remainder of the plant material was dried, ground, and stored for chemical analysis.

2.2. DMG solution testing

Previous studies (e.g. L'Huillier et al., 1996; Heath et al., 1997; Sagner et al., 1998; Küpper et al., 2001; Boominathan and Doran, 2003; Mizuno et al., 2003; Seregin et al., 2003; Bhatia et al., 2004) examined a wide range of DMG solvents for Ni staining in plant tissues. We tested five solutions: Three solutions were used as described in the literature; two were obtained by modification of proposed solutions (Table 1). The solution containing borax and KOH is a modification of the borax/NaOH solution used by Seregin et al. (2003). The reason for this replacement was that plant tissues tolerate potassium (K) better than sodium (Na) (Mäser et al., 2002; Rodriguez-Navarro and Rubio, 2006). High Na contents may destroy cells due to osmotic pressure and thus lead to Ni redistribution.

Cross-sections were cut by means of a manual cylinder microtome (Dr. G. Schuchardt, Göttingen). To compare the effects of the different solutions, we applied 30 μl droplets on ~150 μm thick cross-sections of leaf, stem and root tissues from plants grown in 125 and 250 mg Ni kg^{-1} soil. The maximum distance between two cross-sections stained with different DMG solutions was 5 mm to keep the variation between sections as small as possible. We added <30 μl of solution to each cross-section to minimise leaching. We photographed the stained sections with 100× magnification some

Table 1
DMG solvents tested.

Solvent	Proposed by	Composition of DMG-solution	Tested plants and plant parts	pH	Optical detection limit of Ni	DMG solubility
KOH	Boominathan and Doran (2003)	1.16 g DMG dissolved in 100 ml 0.1 M KOH solution	*Alyssum bertolonii* (roots)	12	2 mg l^{-1}	Low
Ethanol	Küpper et al. (2001)	1% DMG (w/v) dissolved in ethanol	*Alyssum lesbiacum* (leaves)	8.4	2 mg l^{-1}	Soluble after 2h of shaking
Ethanol/amm. ac.	Mizuno et al. (2003)	1 g DMG added to 100 ml ethanol and mixed with 1 M ammonium acetate solution (1:5)	*Thlaspi japonicum* (leaves)	6.9	4 mg l^{-1}	Well
Borax/NaOH	After Seregin et al. (2003)	1 g DMG and 1.5 g NaOH dissolved in 100 ml of 0.05 M $Na_2B_4O_7 \cdot 10H_2O$ solution	*Zea mays* L. (roots)	13	2 mg l^{-1}	Well
Borax/KOH	After Boominathan and Doran (2003) and Seregin et al. (2003)	1 g DMG and 0.18 g KOH dissolved in 100 ml of 0.025 M $Na_2B_4O_7 \cdot 10H_2O$ solution		10	2 mg l^{-1}	Low

30 s after the application of the solution to the sections, using a light microscope (Zeiss, Switzerland) fitted with a digital camera (Canon Power Shot A640). The time between sample preparation and photography was kept as short as possible to avoid dehydration and formation of Ni–DMG crystals. For each solution, we measured the pH and quantitatively determined the solubility of DMG in the solvents after 2 h of shaking. The optical detection limits of Ni for the five solvents were compared by adding a droplet of each solution and a droplet of a Ni-standard solution on a white filter paper. This procedure was repeated with increasingly diluted Ni-solutions (12–1 mg l^{-1}) until there was no red colouration visible (Seregin et al., 2003).

2.3. Sampling and preparation of the specimens

As described in Section 3.1, the borax/KOH solution (Table 1) was found to be the most suitable DMG solvent. This solvent was subsequently used for all further tests. For these tests, *B. coddii* were grown, sampled and prepared for DMG staining as described above. Three leaves were sampled from each plant (the first fully developed leaf on top, fourth leaf from top and bottom leaf): From each leaf, three cross-sections were taken (tip, middle, and one close to the base). Roots were washed with deionised water and one root of average thickness was chosen for cross-sectioning. One cross-section was taken close to the shoot and one in the middle of the roots. In addition, two cross-sections were taken from the stem of each plant (top and middle).

2.4. Image analysis

2.4.1. Karhunen–Loeve transformation

The colour images obtained by the digital camera were recorded in the RGB colour space, i.e. in the three colour channels red, green, and blue. To separate DMG from non-DMG signals, e.g. from chlorophyll, we inspected collocation histograms for the three colour channel combinations red–green, red–blue, and green–blue. The red–green combination showed distinct clusters, and therefore represented the best choice for separation of DMG from other signals. We used the Karhunen–Loeve transformation (Jain, 1989; Basso et al., 2010) to separate the colours representing chlorophyll and DMG as much as possible. Using this transformation, two stochastic signals become statistically independent. They are now projectable into orthonormal components, where the independent vectors are red and green. This was achieved by computing the eigenvector matrix $\mathbf{S}$ of the covariance matrix $\mathbf{C} = \mathrm{cov}(\mathbf{I}_{red}, \mathbf{I}_{green})$ for the two colour channels, given by

$$\mathbf{C} = \mathbf{S}\ddot{\mathbf{E}}\mathbf{S}^{\mathrm{T}} \quad (1)$$

$\ddot{\mathbf{E}}$ is the diagonal matrix of the eigenvalues and $\mathbf{I}_{red}$ and $\mathbf{I}_{green}$ are the row vectors of the intensities in the colour channels for red and green. The covariance matrix being symmetric and its eingevectors orthogonal, the eigenvector matrix $\mathbf{S}$ was used to transform the two channels into the matrix

$$\mathbf{K} = \mathbf{S}\begin{pmatrix} \mathbf{I}_{red} \\ \mathbf{I}_{green} \end{pmatrix} \quad (2)$$

The rows of $\mathbf{K}$ contained the independent basis images, which represent the primary signals for chlorophyll and Ni–DMG and projected into an orthonormal real space of orthogonal vectors. The basis image in $\mathbf{K}$ corresponding to the larger of the two eigenvalues contained the Ni concentration information. As a final step, the basis image was reshaped into its original dimension. For all steps of the image processing the program Matlab (MathWorks) was used.

2.4.2. Determination of averaged tissue DMG staining intensities

Before we analysed the intensities of the tissue staining in the processed images, we subtracted the mean background intensity from each single image by measuring the intensity of a rectangular area next to the sample and subtracting it from the total image intensity. Then, we selected 3–5 rectangular areas in each particular tissue and determined the median staining intensities in the areas. The averages of the 3–5 replicate areas were taken as the mean staining intensity in the respective tissues.

2.4.3. Calibration

To convert colour intensities into concentrations (mg Ni kg^{-1} fresh weight), we prepared agar standards as a substitute for plant tissues. Nickel nitrate was added at concentrations of 0, 25, 50, 100, 200, 400, 800, 1600, 3200 mg Ni l^{-1} to a solution of 30 g agar l^{-1}. Such a high agar concentration compared to standard applications for in vitro cultures was needed for the stability of the slides and because of Ni–DMG leaching at lower concentrations. After autoclaving, the Ni-spiked agar solutions were filled into Petri dishes. The final Ni concentrations of the standards were determined by means of ICP-OES.

The agar standards were sectioned and stained in the same way as the plant samples: Cross-sections of ~150 μm were cut, DMG-solution was added, and the samples were imaged using light microscopy. We analysed five replicates of each concentration standard.

After image processing, we fitted a power function to the experimental data in order to describe the relationship between staining intensity and Ni concentration (Eq. (3)). This function was then used to calculate the Ni concentrations of the stained plant tissues of *B. coddii*. The detection limit of the method was set to the lowest Ni concentration in agar that resulted in a staining of the agar that was

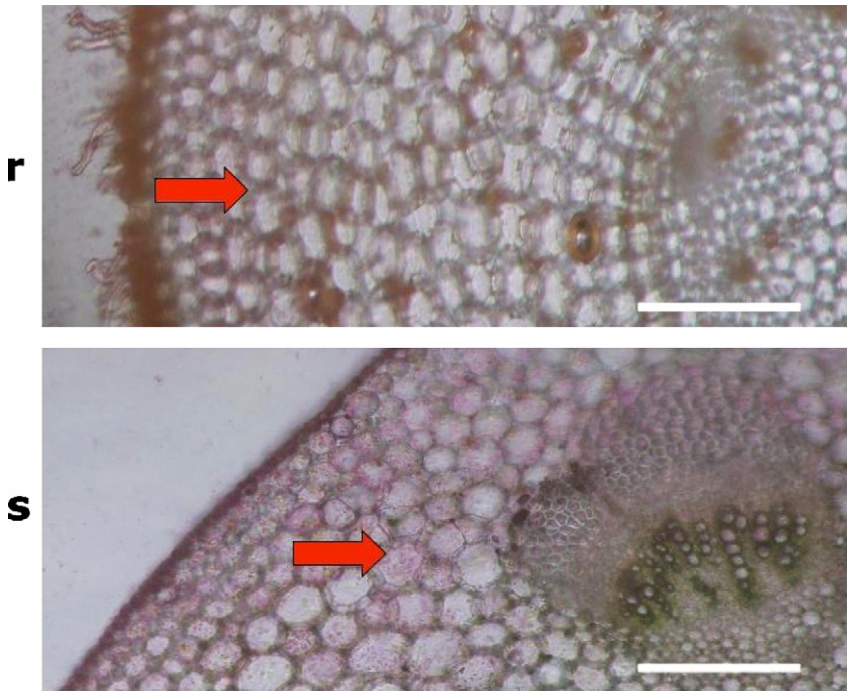

Fig. 1. Distribution of Ni, indicated by the red colouration, in roots (r) and stems (s) of *Berkheya coddii* plants that were grown in soils containing 500 mg Ni kg^{-1} soil. Red arrows show small $Ni(DMG)_2$-cristals in the apoplast (r) and in the symplast (s). White scale bars represent ~250 μm. (For interpretation of the references to colour in this figure legend, the reader is referred to the web version of the article.)

significantly different from the blank agar samples (Wilcoxon rank sum test).

2.5. Validation

2.5.1. ICP-OES measurement

To test the calibration with the agar standards, we also determined the Ni concentrations of plant tissues by means of ICP-OES (Vista-MPX, Varian). To obtain sufficient material for ICP analysis, the leaf sampled for staining was analysed together with its nearest neighbour leaf. For stem samples, the stem was divided into four parts that were analysed separately. The entire root system was analysed because of the small mass of the root samples. The samples were dried for 24 h at 40 °C and then digested for 40 min at 150 °C in 15 ml HNO_3 using a digestion block (DigiPREP MS, SCP-Science). Fresh agar samples were digested in the same way as the plant samples. As we could not find plant reference material with comparable Ni concentrations, we used standard addition with a final Ni concentration of 1 mg l^{-1} in the analysed solution (Ni standard solution, MERCK) for quality control.

2.5.2. Comparison of DMG-staining with ICP-OES analysis

To compare the concentrations determined by ICP-OES with those obtained by DMG-staining, the ICP-measured concentrations were expressed as fresh-weight related concentrations (mg Ni kg^{-1}). Ratios of dry weight/fresh weight were determined separately for leaf, stem and root samples in four replicates each. Fresh weight concentrations were calculated by multiplying the dry weight concentrations with the respective dry weight/fresh weight quotient.

The Ni concentrations obtained by DMG staining related to part of a cross-section only, as it was not possible in general to accurately analyse the entire cross-sectional area for staining intensity. Thus, the values determined by ICP-OES and DMG staining do not exactly relate to the same areas of the cross-sections. For the leaves, we restricted the comparison for this reason to the mid ribs. For roots, we assumed that the average Ni concentrations of the selected cross-sections gave a sufficient approximation for the Ni concentrations determined by the ICP-OES measurements.

2.6. Statistical analysis of the data

For pairwise comparisons of the agar standards, the Wilcoxon rank sum test was used. To analyse the differences in concentration between different plant parts (leaves, stems and roots) and between the different plant tissues, we used one-way ANOVA, followed by pairwise *t*-test (*p*-value adjustment method: holm). The significance level was set at $p \leq 0.05$. All statistical tests were performed using the software package "R", version 2.1 (R Development Core Team, 2008).

3. Results

3.1. Solvent choice

The overall distribution patterns of Ni in the tissues of *B. coddii*, obtained with the five DMG-solutions (Table 1) were similar. However, the image quality differed considerably between solvents. The solution that contained only ethanol evaporated rapidly, and imaging became impossible after 5 min. Moreover, long Ni–DMG crystals formed. The ammonium acetate/ethanol mixture produced a weaker colour than the other solutions, probably because of the lower solution pH. We found no differences between the KOH, the borax/NaOH and the borax/KOH solutions. With all three solutions, we observed development of small crystals 5–10 min after adding the solvents. We chose the borax/KOH solution for all subsequent DMG staining, because (a) the staining produced images of high quality under the light microscope, (b) the pH was optimal for Ni complexation, and (c) plant tissues are generally more tolerant to K than to Na.

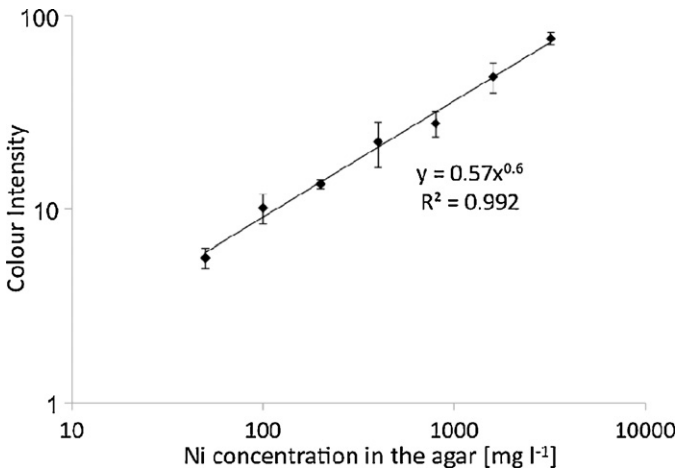

Fig. 2. Ni-agar-standard calibration curve [log–log scale]. The *X*-axis shows the Ni concentrations of the agar medium and the *Y*-axis shows the intensity of the DMG staining after image-processing and background subtraction. Error bars represent the standard errors of the means.

3.2. Qualitative image analysis

At all Ni concentrations applied, intensive DMG staining was detected in the epidermal cells of leaves and stems (data not shown). Elevated staining intensities were also found in the vascular bundles (xylem and phloem) of many samples. In the roots, staining intensity decreased in the cortex from the exodermis towards the stele. The DMG-staining revealed that Ni was present in both the apoplast and the symplast of various root tissues. In the root cortex, we detected the highest staining intensities in the apoplast, whereas in the stems and leaves most of the DMG stain was found within cells (Fig. 1).

3.3. Calibration

The calibration curve obtained with the agar standards (Fig. 2) followed the power function

$$\mathbf{c} = 2.554 * \mathbf{I}^{1.662} \quad (3)$$

where **c** is Ni concentration and **I** is colour intensity.

The intensity of the DMG-staining was less homogeneous in the agar samples with higher Ni concentrations (>200 mg l^{-1}) than in those with lower Ni concentrations. This resulted in larger standard errors at higher concentrations. The intensity of the agar standard with the lowest non-zero Ni concentration (25 mg l^{-1}) was not significantly different from that of blank agar samples. The next Ni concentration level (50 mg l^{-1}), however, differed significantly from the control ($p < 0.01$). This indicates that the detection limit was between 25 and 50 mg Ni l^{-1}. Comparing samples of plants grown in soil with elevated Ni concentrations with those from control soil (background concentration) revealed clear differences in staining intensity (Fig. 3). The differences were visible in all image processing steps: from the raw RGB-images (a1 and b1), through the transformed images (a2 and b2) to the final Ni-concentration maps (a3 and b3). Even though the leaves of *B. coddii* grown in control soil (soil concentration of 18.6 ± 4.3 mg Ni kg^{-1}) only accumulated 10.7 ± 2.5 mg Ni kg^{-1} dry weight, a faint staining was still visible (b2 and b3). This means that the Ni was probably not distributed homogeneously, but accumulated in some parts of the leaves, particularly in the epidermis, at concentrations above the detection limit. Moreover, the colour of the tissue may have interfered slightly with the colour of the Ni–DMG complexes. Light reflection caused by air bubbles occasionally produced colour artefacts that interfered with the colour intensity resulting from Ni–DMG complexation (Fig. 3b3). Image processing worked well for roots, stems and leaf midrib cross-sections. In the leaf blades, the high chlorophyll content of the mesophyll slightly impaired Ni–DMG detection. Fig. 4 gives examples for the patterns of Ni distribution found in the root, stem and leaf samples of the plants grown on soil with 500 mg Ni kg^{-1}.

3.4. Quantitative analysis of Ni distribution patterns

For comparison with the calibrated Ni-DMG concentrations, fresh weight related Ni concentrations were also determined by multiplying the ICP-OES measurements with the respective dry-weight-to-fresh-weight ratios for leaves, stems, and roots. The average values of these ratios from five exemplary samples were

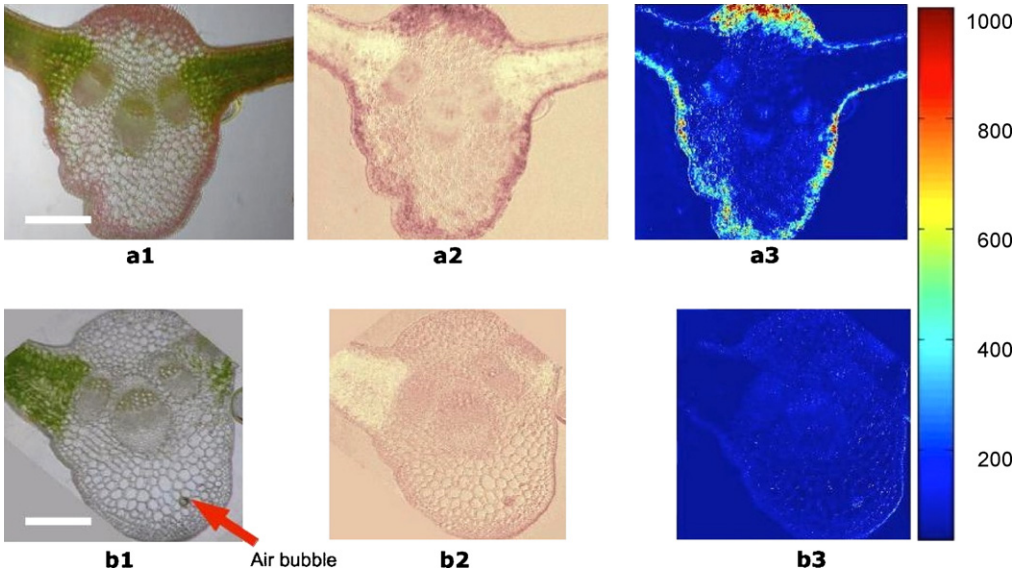

Fig. 3. Image processing steps from the raw RGB-images (a1, b1) to the transformed images (a2, b2) showing intensities and the calibrated concentration maps (a3, b3 [colour bars show mg Ni kg^{-1} fresh weight]). The samples are: (a) a leaf midrib of *B. coddii* grown in a soil containing 250 mg kg^{-1} Ni and (b) leaf midrib from *B coddii* growing on a soil with background Ni concentrations. In the images b1–b3 the artefact is due to air bubble. White scale bars represent distance of ~250 μm. (For interpretation of the references to colour in this figure legend, the reader is referred to the web version of the article.)

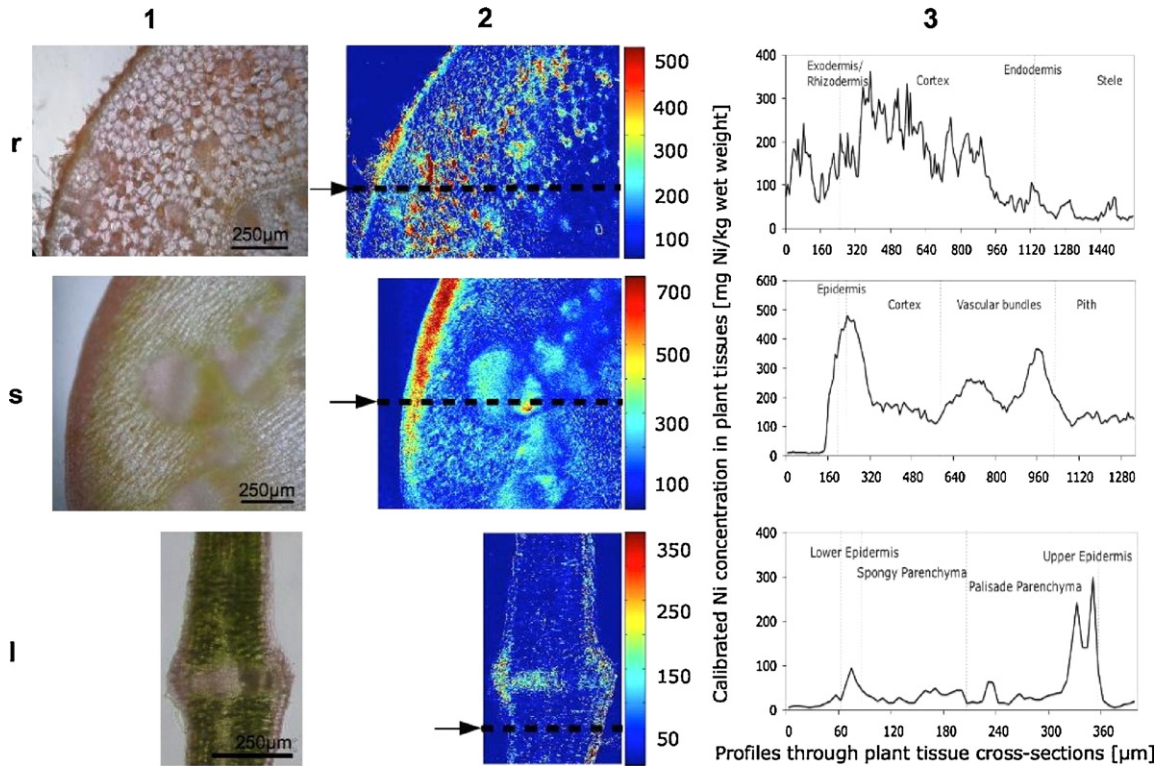

Fig. 4. RGB images of cross-sections of roots, stems and leaves of *B. coddii* (r1, s1, l1) growing on 500 mg kg^{-1} next to their calibrated concentration maps (r2, s2, l2). Arrows in the concentration map images indicate the middle line of a rectangular area of <200 pixel thickness. Mean values of the columns of these rectangular areas were calculated and were subsequently plotted as cross-section profiles (r3, s3, l3).

0.16 ± 0, 0.18 ± 0.03, and 0.18 ± 0.01 for leaves, stems, and roots, respectively. At all soil Ni concentrations, there was a significantly higher ($p < 0.05$) Ni concentration in the leaves than in the stems and roots (Fig. 5). We found the highest concentrations in the lower leaves and upper stems (data not shown), in agreement with Robinson et al. (2003).

Tables 2 and 3 show that the Ni concentrations determined by DMG-staining were systematically lower than the values obtained from the ICP-OES analysis of the respective plant parts. The same trend was found for cross-sections of the middle stem (data not shown). Even though variability among images was high, and considering that the images did not cover entire cross-sections, there was a large discrepancy in the Ni concentrations

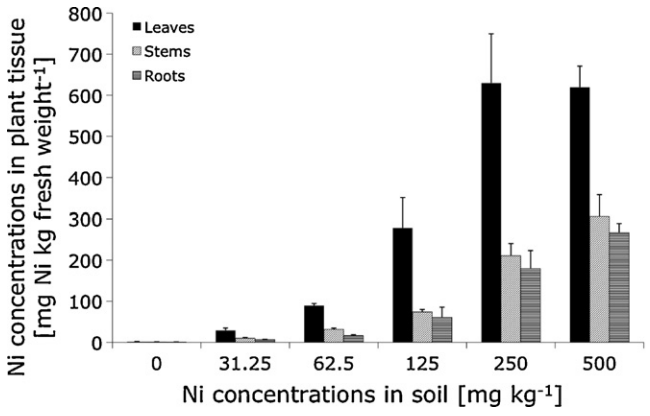

Fig. 5. Average Ni concentration in leaves, stems and roots measured using ICP-OES ($n = 3$). Fresh weight values were calculated from dry weight values multiplied by the dry weight/fresh weight ratio of 0.16 for leaves and 0.18 for stems and roots. Error bars represent the standard errors of the means.

obtained with the two methods. Per unit cross-sectioned area, we detected between 15 and 30% of the Ni detected with the ICP-OES measurement.

Ni concentrations increased with soil Ni concentrations in the epidermis of roots and stems (Table 2). The concentrations of Ni were significantly higher in epidermal and exodermal tissues of shoots and roots after exposure to 250 mg kg^{-1} than to 62 mg kg^{-1} soil Ni ($p < 0.01$). The Ni concentrations of the other tissues were below the detection limit in most samples. In the stems, Ni concentrations were in all samples higher in the epidermis than in the cortex and the pith. The vascular bundles occasionally showed higher Ni accumulation than cortex and pith.

For leaves, we only analysed leaf midrib tissues of plants exposed to 250 mg Ni kg^{-1} soil (Table 3). Here, the DMG–Ni concentrations of the upper epidermis ranged from 329 ± 40 in the top leaves to 400 ± 29 mg Ni kg DW^{-1} in the bottom leaves and from 195 ± 14 to 407 ± 28 mg Ni kg DW^{-1} (top leaves–bottom leaves) for the lower epidermis. This is consistent with our ICP-OES measurements that showed the lowest concentrations in the top leaves and the highest concentrations in the bottom leaves (Table 3). The values obtained for the inner collenchymas and the vascular bundles were in all samples significantly lower than for the upper epidermis ($p < 0.05$). In the top leaves, the lower epidermis showed significantly lower concentrations than the upper epidermis ($p < 0.05$).

4. Discussion

Using DMG to determine Ni distribution patterns in roots, stems and leaves of *B. coddii* gave reproducible results. These patterns were similar to those reported by other authors investigating Ni distribution in *B. coddii* using other methods (Budka et al., 2005; Mesjasz-Przybylowicz et al., 2001; Moradi et al., 2010; Robinson

Table 2
Ni concentrations measured with ICP-OES (ICP) compared to calibrated Ni concentrations in the plant tissues of roots and stems using DMG-staining and image processing (DMG). Values give averages and standard errors ( ) of *n* replicates in mg Ni kg^{-1} fresh plant tissue.

		Ni concentration in soil [mg kg^{-1}]				
		0 *n* = 3	62.5 *n* = 3	125 *n* = 3	250 *n* = 3	500 *n* = 2
ICP	Stem (top)	1.3 (0.1)	42.6 (1.6)	101.7 (10.2)	292.9 (39.0)	350.7 (44.5)
DMG	Stem tissues (top)					
	Epidermis	<50	35.0 (12.2)	103.3 (51.5)	254.6 (25.9)	302.8 (87.2)
	Cortex	<50	<50	<50	<50	89.8 (37.3)
	Vascular bundles	<50	<50	<50	62.5 (42.9)	144.3 (36.4)
	Pith	<50	<50	<50	<50	142.3 (27.7)
ICP	Whole root	0.9 (0.1)	16.4 (1.9)	60.5 (25.0)	179.4 (43.9)	266.8 (22.1)
DMG	Root tissues					
	Exodermis	<50	45.5 (4.3)	68.7 (6.3)	84.3 (5.6)	318.0 (30.0)
	Outer cortex	<50	<50	<50	<50	233.6 (120.8)
	Inner cortex	<50	<50	<50	<50	169.0 (133.0)
	Endodermis	<50	<50	<50	<50	129.7 (101.9)
	Stele	<50	<50	<50	<50	75.1 (75.1)

et al., 2003). As in our study, Budka et al. (2005) found the highest concentrations of Ni in the epidermis and vascular bundles of *B. coddii*. These authors analysed freeze substituted samples using tetrahydrofuran, which may have limited detection to Ni bound to histidine and organic acids such as citrate and malate. The high concentrations we found in midrib epidermis (Table 3) agree with the results of Mesjasz-Przybylowicz et al. (2001).

Using laser ablation to investigate the distribution of Ni in the roots of *B. coddii*, Moradi et al. (2010) found the lowest root Ni concentrations in the stele, as we found here. In contrast to the DMG method used in our study, the spatial resolution of the laser ablation method was insufficient to distinguish between exodermis and cortex. Similar Ni distribution patterns were also found in the roots of other Ni hyperaccumulators. Mesjasz-Przybylowicz et al. (2007) found that the concentrations of Ni decreased from the outer cortex towards the inner cortex also in the roots of another Ni hyperaccumulator plant (*Senecio coronatus Harv*). Bhatia et al. (2004) found higher Ni concentrations in the vascular bundles than in the cortex and pith in *Stackhousia tryonii F.M. Bailey*. High Ni-concentrations in epidermal tissues was reported for *Alyssum bertolonii Desv.* by Marmiroli et al. (2004) and for *Stackhousia tryonii F.M. Bailey* by Bhatia et al. (2004). For other plant species, different Ni distribution patterns were observed. Berazain et al. (2007) found the highest Ni concentrations in the cortex of the stems of six species of the *Euphorbiaceae* family. Differences in reported Ni distribution patterns between different plants, however, may also be due to differences in the methods, plant cultivation or the age of the analysed tissues (Smart et al., 2007). Berazain et al. (2007) used EDXA, which may respond differently to less soluble Ni fractions than DMG.

The observation of Ni in the phloem of leaves and stems indicates that Ni in *B. coddii* is redistributed from older to younger leaves through phloem transport (Marschner, 1986; Page and Feller, 2005; Riesen and Feller, 2005). This would also explain the high Ni concentration Mesjasz-Przybylowicz et al. (2001) found in young *B. coddii* leaves.

The variation in Ni concentrations in our images may be due to (1) natural physiological variability in Ni accumulation, (2) variation in cross-section thickness, and (3) variations in light conditions. Variations in thickness of the cross-sections could be substantially reduced by using an automatic microtome instead of a manual microtome. For a given type of tissue, the influence of thickness variations may be reduced to some degree by normalization with respect to chlorophyll content or another component provided it has a homogenous distribution. The effect of light variation can be corrected by subtracting background values. Keeping light conditions constant is a crucial point in the method. Interferences of air bubbles and chlorophyll with the DMG colour are other challenges in DMG staining. Air bubbles can form at any time and any part of the sample, and they are difficult to eliminate during sample preparation. Light reflection and scattering of air bubbles interfere with those of the Ni–DMG complexes. High chlorophyll contents may reduce DMG colour-contrasts in particular in leaf blade sections. The separation of DMG–Ni and chlorophyll signals may be further improved by a more sophisticated image analysis.

The DMG method systematically gave lower tissue Ni concentrations than HNO_3 digestion and ICP-OES analysis. This indicates that DMG-stained Ni did not represent all tissue Ni, most likely because part of the Ni was not available to react with DMG. As the stability of Ni–DMG complexes is high with a log K of 14.6 (Furia,

Table 3
Ni concentrations in leaves measured with ICP-OES (ICP) compared to calibrated Ni concentrations in leaf midrib tissues using DMG-staining and image processing (DMG). Values give averages and standard errors ( ) of *n* replicates in mg Ni kg^{-1} fresh plant tissue.

		Ni concentration in soil [mg kg^{-1}]: 250 mg kg^{-1}		
		Bottom leaves *n* = 3	Middle leaves *n* = 3	Top leaves *n* = 3
ICP	Whole leaves	683.1 (150.2)	667.6 (115.6)	538.4 (97.9)
DMG	Leaf midrib tissues			
	Upper epidermis	400.2 (28.3)	318.8 (25.6)	329.1 (39.5)
	Upper outer collenchyma	333 (57.0)	207.1 (40.8)	207.5 (55.9)
	Upper inner collenchyma	221.6 (31.2)	52.4 (9.8)	103.4 (6.3)
	Vascular bundles	102.2 (34.1)	73.8 (15.4)	54.9 (6.1)
	Lower inner collenchyma	161.9 (32.6)	<50	70.2(17.5)
	Lower outer collenchyma	254.5 (17.6)	157 (50.8)	180.7 (4.3)
	Lower epidermis	406.5 (28.1)	245.8 (46.4)	195(13.5)

1972), it can be assumed that all Ni ions that are physically accessible by DMG in a plant tissue will be detected. The stability constant of $Ni(DMG)_2$ for example is higher than that of Ni with histidine or that with citric acid (log K of 8.69 and 4.8, respectively), which are both important ligands for Ni in plant tissues (Krämer et al., 1996; Haydon and Cobbett, 2007). However, DMG may not be able to complex all Ni bound in walls, because the DMG solution may not penetrate suberin and wax containing structures (Smart et al., 2007). Another source of error for underestimation of Ni concentrations in the DMG method compared to ICP-OES analysis could be the use of agar as a medium representing plant tissue in the calibration procedure. It is likely that the speciation of Ni in agar is distinct from that in plant tissue.

The DMG method developed here has particular potential to be used for comparative analyses of Ni distribution pattern in cross-sections, where factors such as the thickness of sections can be kept constant or do not play a great role. For example, the method can reveal whether Ni is stored in the apoplast or in the symplast (Fig. 1). Such observations can provide important information about uptake processes and underlying mechanisms. The finding that in the root cortex Ni was concentrated in the apoplast indicates that Ni is transported along the apoplastic pathway until reaching the endodermis (Marschner, 1986). The advantage of our DMG-staining method is that cross-sections can be imaged immediately after the addition of the DMG-solution. This means that there is little time available for redistribution of Ni or crystal formation, a problem of methods that involve soaking of cross-sections in DMG-solutions for several hours (Mizuno et al., 2003; Bhatia et al., 2004). The low costs of this method and its simplicity make it widely applicable.

5. Conclusions

Using a borax/KOH/DMG solution with a pH of 10, we obtained consistent and reproducible DMG-staining patterns of tissue sections of the Ni hyperaccumulator *B. coddii*, revealing how Ni that is accessible to the stain is distributed in this plant. To obtain optimal results it is necessary that sections be imaged immediately after staining. It appears that a substantial Ni fraction in the tissues is not accessible to the stain, possibly because it is unable to penetrate suberin and wax-containing structures such as cell walls. The observed distribution patterns were in good agreement with the findings of other authors using different methods. The DMG-staining method has the advantage that it gives a good spatial resolution, does not require expensive equipment, is easy to use, and is rapid in comparison to other methods.

References

Andreĭ, O., Vollenweider, P., Günthardt-Goerg, M.S., 2006. Foliage response to heavy metal contamination in sycamore maple (*Acer pseudoplatanus* L.). Forest Snow Landscape Research 80 (3), 275–288.

Basso, A., Cavagnino, D., Pomponiu, V., Vernone, A., 2010. Blind watermarking of color images using Karhunen–Loève transform keying. The Computer Journal, doi:10.1093/comjnl/bxq052.

Berazain, R., de la Fuente, V., Rufo, L., Rodriguez, N., Amils, R., Diez-Garretas, B., Sanchez-Mata, D., Asensi, A., 2007. Nickel localization in tissues of different hyperaccumulator species of euphorbiaceae from ultramafic areas of Cuba. Plant Soil 293, 99–106.

Bhatia, N.P., Walsh, K.B., Orlic, I., Siegele, R., Ashwath, N., Baker, A.J., 2004. Studies on spatial distribution of nickel in leaves and stems of the metal hyperaccumulator *Stackhousia tryonii* using nuclear microprobe (micro-PIXE) and EDXS techniques. Functional Plant Biology 31, 1061–1074.

Bidwell, S.D., Crawford, S.A., Woodrow, I.E., Sommer-Knudsen, J., Marshall, A.T., 2004. Sub-cellular localization of Ni in the hyperaccumulator, *Hybanthus floribundus* (Lindley) F. Muell. Plant, Cell and Environment 27, 705–716.

Boominathan, R., Doran, P.M., 2003. Organic acid complexation, heavy metal distribution and the effect of ATPase inhibition in hairy roots of hyperaccumulator plant species. Journal of Biotechnology 101, 131–146.

Boyd, R.S., 1998. Hyperaccumulation as a plant defensive strategy. In: Brooks, R.R. (Ed.), Plants that Hyperaccumulate Heavy Metals. CAB INTERNATIONAL, pp. 181–201.

Brooks, R.R., 1977. Detection of nickeliferous rocks by analysis of herbarium species of indicator plants. Journal of Geochemical Exploration 7, 49–57.

Brooks, R.R., 1987. Serpentine and Its Vegetaion: A Multidisciplinary Approach. Dioscorrides, Portland, Oregan, USA.

Brooks, R.R., 1998a. General introduction. In: Brooks, R.R. (Ed.), Plants that Hyperaccumulate Heavy Metals. CAB INTERNATIONAL, pp. 1–14.

Brooks, R.R., 1998b. Geobotany and hyperaccumulators. In: Brooks, R.R. (Ed.), Plants that Hyperaccumulate Heavy Metals. CAB INTERNATIONAL, pp. 55–94.

Budka, D., Mesjasz-Przybylowicz, J., Tylko, G., Pryzbylowicz, W.J., 2005. Freeze substitution methods for Ni localization and quantitative analysis in *Berkheya coddii* leaves. Nuclear Instruments and Methods in Physics Research B 231, 338–344.

Dakhel, A.A., Ali-Mohamed Ahmed, Y., Henari, F.Z., 2006. Structural and optical studies of evaporated bis-(dimethylglyoximato)nickel(II) thin films. Optical Materials 28, 925–929.

Furia, T.E., 1972. Sequestrants in foods. In: CRC Handbook of Food Additives, 2nd ed. CRC Press, Cleveland, OH (Chapter 6).

Haydon, M.J., Cobbett, C.S., 2007. Transporters of ligands for essential metal ions in plants. New Phytologist 174, 499–506.

Heath, S.M., Southworth, D., D'Allura, J.A., 1997. Localization of nickel in epidermal subsidiary cells of leaves of *Thlaspi montanum* var. Siskiyouense (Brassicaceae) using energy-dispersive X-ray microanalysis. International Journal of Plant Sciences 158 (2), 184–188.

Jain, A., 1989. Fundamentals of Digital Image Processing. Prentice Hall, ISBN 0-13332578-4.

Krämer, U., Cotter-Howells, J.D., Chanrock, J.M., Baker, A.J., 1996. Free histidine as a metal chelator in plants that accumulate nickel. Nature 379, 635–638.

Küpper, H., Lombi, E., Zhao, F.-J., Wieshammer, G., McGrath, S.P., 2001. Cellular compartmentation of nickel in the hyperaccumulators *Alyssum lesbiacum*, *Alyssum bertolonii* and *Thlaspi goesingense*. Journal of Experimental Botany 52 (365), 2291–2300.

L'Huillier, L., d'Auzac, J., Durand, M., Michaud-Ferriere, N., 1996. Nickel effects on two maize (*Zea mays*) cultivars: growth, structure Ni concentration and localization. Canadian Journal of Botany 74, 1547–1554.

Marmiroli, M., Gonelli, C., Maestri, E., Gabbrielli, R., Marmiroli, N., 2004. Localisation of nickel and mineral nutrients Ca, K, Fe, Mg by scanning electron microscopy microanalysis in tissues of the nickel-hyperaccumulator *Alyssum bertolonii* and the nonhyperaccumulator *Alyssum montanum* l. Plant Biosystems 138 (3), 231–243.

Marschner, H., 1986. Mineral Nutrition of Higher Plants, 2nd ed. Academic Press Limited.

Mäser, P., Gierth, M., Schröder, J., 2002. Molecular mechanisms of potassium and sodium uptake in plants. Plant and Soil 247, 43–54.

McNear, D.H., Peltier, E., Everhart, J., Chaney, R.L., Sutton, S., Newville, M., Rivers, M., Sparks, D.L., 2005. Application of quantitative fluorescence and absorptionedge computed microtomography to image metal compartmentalization in *Alyssum murale*. Environmental Science Technology 39, 2210–2218.

Mesjasz-Przybylowicz, J., Barnabas, A., Pryzbylowicz, W.J., 2007. Comparisons of cytology and distribution of nickel in roots of Ni-hyperaccumulating and non-hyperaccumulating genotypes of *Senecio coronatus*. Plant Soil 293, 61–78.

Mesjasz-Przybylowicz, J., Pryzbylowicz, W.J., Pineda, C.A., 2001. Nuclear microprobe studies of elemental distribution in apical leaves of the Ni hyperaccumulator *Berkheya coddii*. South African Journal of Science 97, 591–593.

Migliorini, M., Pigino, G., Bernini, F., Leonzio, C., 2004. The effects of heavy metal contamination on the soil arthropod community of a shooting range. Environmental Pollution 129, 331–340.

Mizuno, N., Nosako, S., Mizuno, T., Horie, K., Obata, H., 2003. Distribution of Ni and Zn in the leaves of *Thlaspi japonicum* growing on ultramafic soil. Soil Science and Plant Nutrition 49 (1), 93–97.

Moradi, A.B., Swoboda, S., Prohaska, T., Robinson, B.H., Kästner, A., Oswald, S., Wenzel, W.W., Schulin, R., 2010. Mapping of nickel in root cross-sections of the hyperaccumulator plant *Berkheya coddii* using laser ablation ICP-MS. Environmental and Experimental Botany 69, 24–31.

Ortega, R., 2005. Chemical elements distribution in cells. Nuclear Instruments and Methods in Physics Research B 231, 218–223.

Ozturk, L., Yazici, M.A., Yucel, C., Torun, A., Cekic, C., Bagci, A., Ozkan, H., Braun, H.-J., Sayers, Z., Cakmak, I., 2006. Concentration and localization of zinc during seed development and germination in wheat. Physiologia Plantarum 128, 144–152.

Page, V., Feller, U., 2005. Selective transport of zinc, manganese, nickel, cobalt and cadmium in the root system and transfer to the leaves in young wheat plants. Annals of Botany 96, 425–434.

R Development Core Team (2008). R: A Language and Environment for Statistical Computing. R Foundation for Statistical Computing, Vienna, Austria. ISBN: 3-900051-07-0, URL http://www.R-project.org.

Richau, K.H., Kozhevnikova, A.D., Seregin, I.V., Vooijs, R., Koevoets, P.L.M., Smith, J.A.C., Ivanov, V.B., Schat, H., 2009. Chelation by histidine inhibits the vacuolar sequestration of nickel in roots of the hyperaccumulator *Thlaspi caerulescens*. New Phytologist 183, 106–116.

Riesen, O., Feller, U., 2005. Redistribution of nickel, cobalt, manganese, zinc and cadmium via the phloem in young and maturing wheat. Journal of Plant Nutrition 28 (3), 421–430.

Robinson, B.H., Brooks, R.R., Howes, A.W., Kirkman, J.H., Gregg, P.E.H., 1997. The potential of the high-biomass nickel hyperaccumulator *Berkheya coddii* for

phytoremediation and phytomining. Journal of Geochemical Exploration 60, 115–126.
Robinson, B.H., Lombi, E., Zhao, F.J., McGrath, S.P., 2003. Uptake and distribution of nickel and other metals in the hyperaccumulator *Berkheya coddii*. New Phytologist 158, 279–285.
Rodriguez-Navarro, A., Rubio, F., 2006. High-affinity potassium and sodium transport systems in plants. Journal of Experimental Botany 57 (5), 1149–1160.
Sagner, S., Kneer, R., Wanner, G., Cosson, J.-P., Dues-Neumann, B., Zenk, M.H., 1998. Hyperaccumulation, complexation and distribution of nickel in *Sebertia acuminata*. Phytochemistry 47 (3), 339–347.
Seregin, I.V., Kozhevnikova, A.D., Kazyumina, E.M., Ivanov, V.B., 2003. Nickel toxicity and distribution in maize roots. Russian Journal of Plant Physiology 50 (5), 793–800.
Smart, K.E., Kilburn, M.R., Salter, C.J., Smith, J.A.C., Grovenor, C.R.M., 2007. NanoSIMS and EPMA analysis of nickel localisation in leaves of the hyperaccumulator plant *Alyssum lesbiacum*. International Journal of Mass Spectroscopy 260, 107–114.
Tung, G., Temple, P.J., 1996. Histochemical detection of lead in plant tissues. Environmental Toxicology and Chemistry 15 (6), 906–914.